POLITECNICO
MILANO 1863

DIPARTIMENTO DI MECCANICA

mecc

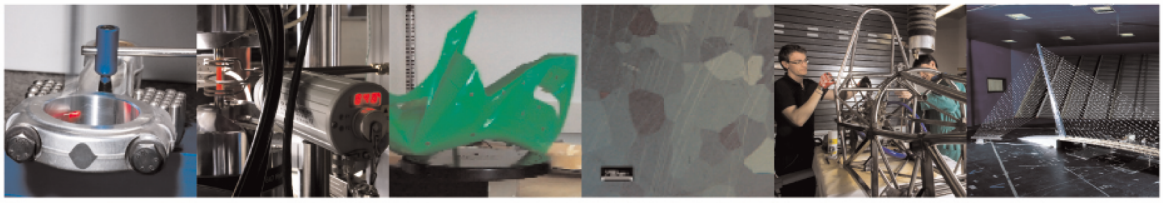

Semi-Active Control of Primary Suspensions to Improve Ride Quality in a High-Speed Railway Vehicle

Bin Fu, Binbin Liu, Egidio Di Gialleonardo, Stefano Bruni

This is an Accepted Manuscript of an article published by Taylor & Francis in *Vehicle System Dynamics* on 10/10/2022, available online:
https://www.tandfonline.com/doi/full/10.1080/00423114.2022.2128827

This content is provided under CC BY-NC-ND 4.0 license

DIPARTIMENTO DI MECCANICA ■ POLITECNICO DI MILANO
via G. La Masa, 1 ■ 20156 Milano ■ EMAIL (PEC): pecmecc@cert.polimi.it
http://www.mecc.polimi.it
Rev. 0

Semi-Active Control of Primary Suspensions to Improve Ride Quality in a High-Speed Railway Vehicle

Bin Fu, Binbin Liu, Egidio Di Gialleonardo, Stefano Bruni*

Dipartimento di Meccanica, Politecnico di Milano, Via La Masa 1, Milano, 20156, Italy

** bin.fu@polimi.it*

Abstract: Semi-active suspensions are seen as a promising technology to improve ride quality in high-speed railway vehicles as they provide substantial benefits not achievable through an optimisation of the passive suspension while avoiding some drawbacks of full-active control. Previous works showed that semi-active primary suspensions (SAPS) offer significant improvement of ride quality. However, published implementations of this concept did not consider the coupling effects between car-body and bogie vibrations, which play a decisive role in the success of control strategies for SAPS. This paper provides a comprehensive analysis of SAPS to improve vehicle ride comfort, with special attention to the mitigation of car-body bending vibration. A vehicle model considering the coupling of car-body bending and bogie pitch is proposed and used for the synthesis of an LQG controller. The performance of the semi-active suspension and controller is assessed using a detailed flexible multibody system of a high-speed vehicle. The proposed control scheme is shown to be highly effective in reducing car-body vibration in the entire frequency range of interest from 1Hz to20Hz. A remarkable ride comfort improvement is found in the entire speed range from 150 km/h to 350 km/h.

Keywords: Semi-active primary suspension, car-body bending, LQG control, vertical ride comfort

1 Introduction

Among different transportation systems, railways are widely recognised as particularly suited to address present environmental challenges in terms of energy savings and reduction of the carbon footprint. One present trend of research, aimed to further increase the environmental friendliness of railways, is to reduce the weight of vehicles through the adoption of new lightweight materials and the structural optimisation of subsystems such as bogies and car-bodies. One undesired effect of having leaner and lighter bodies in railways is that higher levels of structural vibration can be expected, which may affect ride quality and the durability of components. This issue is particularly serious in regard to the

design of car-bodies for high-speed (HS) vehicles. With the decrease of their mass, car-bodies become more flexible and their lowest natural frequencies fall in a frequency range below 20 Hz, in which the human body is highly sensitive to structural vibration [1]. Resonant effects caused by special wavelengths in track irregularities and by the spacing of the axles in the vehicle may take place at relatively high running speeds and are known to affect seriously ride quality [2,3]. These effects can be hardly mitigated through a proper design of passive secondary suspensions, because these are mostly intended to isolate the rigid motion of the car-body from the bogies, and thus secondary suspensions, especially when consisting of air springs, cannot provide the pass-band required to affect the structural resonances of the car-body. Therefore, an interesting alternative is represented by the use of semi-active suspensions which can be highly effective and, at the same time, are significantly less complex and less expensive compared to full-active suspensions.

Past research addressing the mitigation of car-body structural vibration by means of passive solution or mechatronic suspensions is summarized below. Dumitriu proposed to use passive anti-bending bars rigidly fixed onto the car-body frame to increase the car-body bending frequency out of the most interested frequency range, and her numerical analysis showed improved vertical ride indexes [4]. You et al. proposed the use of multiple passive dynamic vibration absorbers (DVA) to reduce the level of vibration of car-body floor in HS vehicles [5]. Goodall investigated full-active and semi-active secondary vertical suspensions to mitigate car-body rigid vibration, showing reduced root mean square of car-body acceleration in numerical simulation [6]. The KTH railway group together with Bombardier performed online tests for full-active secondary suspension on Regina 250, and succeeded in suppressing both rigid and flexible vibration of the car-body using a simple Skyhook control strategy [7]. Foo introduced an actively-controlled mass-spring-damper structure attached to the car-body which proves effective to suppress the bending vibration [8]. Similarly, Huang proposed to improve car-body bending vibration by optimizing the passive suspension for the electric converter suspended under the car-body [9], and then Wang used semi-active suspension to replace the passive components for the suspended system[10]. In the two latter studies, the car-body diamond mode was found to resonate at a frequency close to that of bogie hunting motion, leading to degraded ride comfort [11,12]. The DVA attached to the bogie is designed to move the frequency of hunting motion away from the frequency of car-body diamond mode, and thus to improve the ride comfort [11]. Another attempt by Gong focuses on the optimization of design parameters associated with the vehicle's hunting motion including wheel rail contact geometry, yaw dampers and primary suspension in lateral and longitudinal directions, showing that these measures also

provide mitigation of car-body flexible vibration [12].

This paper focusses on an alternative approach, named semi-active primary suspension (SAPS), with the passive primary vertical dampers being replaced by semi-active dampers. This solution was firstly investigated by Sugahara [13–15] and then by the authors of this paper [16,17], showing significant benefits on ride quality, despite one would expect semi-active secondary suspensions to be better suited to address ride comfort issues. The control strategies proposed for SAPS range from Skyhook [13,17] to model-based techniques, particularly LQG and H∞ [14,16]. Model-based control strategies proposed so far are all defined considering a simple model of the vehicle having 7 degrees of freedom (DOF) [13, 16] which is not considering the coupling of bogie pitch to car-body bending. This model can be considered sufficiently realistic for railway vehicles designed for conventional service but can be highly inadequate to represent HS vehicles equipped with stiff yaw dampers and traction links, as these components provide a strong coupling of car-body bending to bogie pitch. It can be concluded that a comprehensive understanding of control strategies for SAPS is still lacking, especially for HS vehicles, and it is the aim of this paper to provide a contribution in this direction, showing that satisfactory performance of LQG control for SAPS can be achieved using a better suited model of the vehicle in the design of the controller and for state observation.

To this aim, the following new contributions are provided: (i) A comprehensive description of the working mechanism of SAPS is provided, considering the coupling between car-body bending and different components of bogie motion. (ii) A new simplified vehicle model is built which can better represent the vibrational behaviour of the vehicle compared to the one found in the literature while being sufficiently simple to allow the development of model-based controllers in a real application. (iii) The LQG controller synthesised using the new vehicle model scheme is capable of mitigating vehicle vibration not only in relation to the first car-body bending mode (like in [14,16]), but also in relation to the rigid modes of the car-body, showing an excellent capability to improve ride quality in the entire frequency range of interest. (iv) The design of the improved controller is validated using a flexible multibody system (FMBS) of the vehicle, considering in detail car-body flexibility effects.

This paper considers a trailer car in a high-speed trainset, with maximum service speed 350km/h, running on a high-speed line with slab track. From simulations performed using the FMBS model, significant car-body vibration is found especially when the vehicle runs at 230km/h which corresponds to a bending resonance of the car-body at 11.8 Hz. Therefore,

the controller is designed initially to improve the ride quality at 230 km/h, and then the analysis is extended to consider the effect of vehicle speed in the whole speed range 150-350 km/h.

The paper is organised as follows: Section 2 explains the mechanism of the structural coupling between car-body bending and bogie vibrations. Section 3 presents two mathematical models of the railway vehicle considering the above mentioned coupling effect: a simplified 7-DOF model and a detailed FMBS model defined in SIMPACK. Section 4 presents the model-based LQG controller synthesised based on the 7-DOF Coupling model. The effect of SAPS on mitigating car body is analysed in Section 5 by means of simulations performed using the FMBS model.

2 Structural coupling of car-body bending and bogie vibrations

This section provides an overview of the coupling effects between car-body bending modes and bogie vibration, as these effects play a fundamental role in the vibrational behaviour of the vehicle and shall be carefully considered in the design of the controller for the semi-active primary suspension.

The classic 7-DOF vehicle vertical model used in previous studies e.g. [3,14,16] is shown in Fig. 1. The model considers car-body bounce (Z_c) , pitch (θ_c) and first bending mode (q), together with bounce (Z_{t1}, Z_{t2}) and pitch (θ_{t1}, θ_{t2}) for the two bogies.

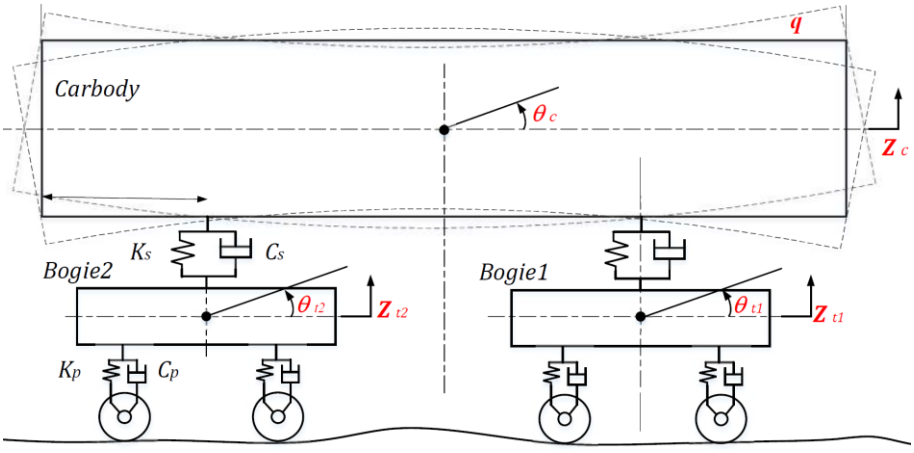

Fig. 1 Classic 7-DOF vehicle vertical model

The model considers the coupling between the first bending mode of the car-body and bogie bounce motion. However, the pitch motion of the bogies has no effect on the deformation of the secondary suspension and hence this model misses all effects related to the coupling of bogie pitch to car-body vibration, whilst these effects can be important especially for HS vehicles [17,18].

As shown in Fig. 2, car-body bending causes a longitudinal displacement δ_x at the positions

where traction links and yaw dampers are connected to the car-body. As a result, the longitudinal forces generated in the traction links and yaw dampers by bogie pitch and longitudinal motion affect the bending vibration of the car-body.

Assuming small bending displacements of the car-body and according to Euler-Bernoulli beam theory, the expression of δ_x is:

$$\delta_x = d_s \frac{\partial w(x,t)}{\partial x} \tag{1}$$

with $w(x,t)$ the bending displacement of the car-body and d_s the distance from the bending neutral layer to the mount point of the yaw dampers or tractions links. The equation governing the bending displacement $w(x,t)$ is introduced in Section 3.2.2.

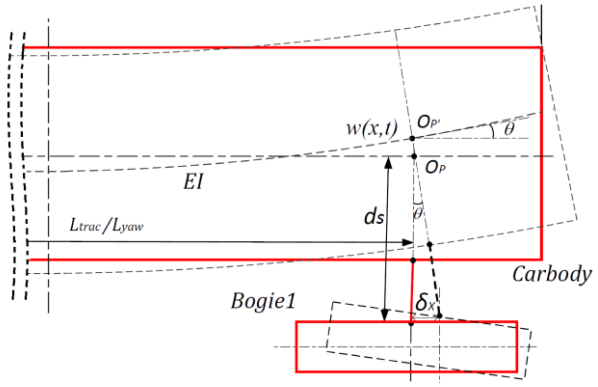

Fig. 2 Coupling effect between car-body bending and bogie pitch, longitudinal motions

It should be noted that the secondary pneumatic suspension, which is the other component connecting the car-body to the bogies has negligible effect on the coupling between car-body bending and bogie pitch and longitudinal motion, because the horizontal stiffness of the air springs is approximately two orders of magnitude lower than the stiffness of the traction links and of the yaw dampers. The coupling between car-body bending and different components of bogie motion is further illustrated using results from the FMBS vehicle model, see Section 3.1.1. These coupling effects need to be properly taken into account in the design of the controller, hence an enhanced 7-DOF model is introduced in Section 3.2.1 and is then used in the synthesis of the controller and for state estimation to implement LQG control.

3 Mathematical models of the railway vehicle

Two mathematical models of the railway vehicle under study are developed:

i.) a flexible multi-body systems (FMBS) model representing in detail the dynamic behaviour of the vehicle in a frequency range up to 30 Hz, including effects of car-

body flexibility, based on a modal synthesis of a 3D finite element model of the car-body. This model is used to assess car-body vibration and ride quality indexes for the passive vehicle and the vehicle equipped with SAPS. The FMBS model is developed in SIMPACK and described in detail in Section 3.1;

ii.) a simplified 7-DOF model which is used in the synthesis of the LQR regulator and also for state estimation using a Kalman filter in the implementation of LQG control. Two different versions of the simplified 7-DOF model are considered: one corresponding to the classic 7-DOF model (see Fig. 1) as a reference, and the newly developed one called 7-DOF-Coupling model (see Fig. 5) which considers the additional coupling effects between the car-body and bogie vibration described in Section 2. The simplified model is developed in MATLAB and described in detail in Section 3.2.

3.1 FMBS vehicle model

The FMBS vehicle model, defined in software SIMPACK, considers one trailed vehicle with one car-body, two bogie frames, four wheelsets, a converter box elastically suspended under the car-body and other smaller bodies being part of the suspensions such as axle-boxes, traction arms (connecting the bogies to the axle-boxes) and traction links (connecting the bogies to the car-body). All bodies are modelled as rigid with 90 DOFs, except the car-body for which flexibility effects are considered through a modal synthesis of a finite element model of the car-body. The cut-off frequency of the finite element model is set to 30 Hz approximately, so that the dynamics of the system can be considered in the whole frequency range relevant to the evaluation of ride quality. Elastic and dissipative effects in suspension components are modelled using non-linear stiffness and damping elements defined based on piecewise linear force vs. deformation or force vs. velocity curves.

A non-linear description of wheel/rail contact is included in the model, considering S1002 wheel profiles and UIC60 rail profiles. Dynamic excitation caused by track irregularities is considered using measured spatial profiles of irregularity from a line equipped with a slab track. These profiles show a distinctive wavelength of longitudinal level irregularity at 5.45 m, corresponding to the spacing of the slabs.

3.1.1 Coupling of car-body bending and bogie vibration in the FMBS model

A modal analysis of the FMBS model was performed in SIMPACK, to determine the natural frequencies and related mode shapes mostly affected by car-body bending and their coupling with the motion of the bogies, as this coupling plays a fundamental role in

determining passengers' comfort. The results are shown in Fig. 3: four modes associated with car-body bending are found with natural frequencies 8.0Hz, 8.8Hz, 10.9Hz and 11.8Hz. The first one show mainly a coupling to bogie bounce motion and the other three modes show a coupling between car-body bending and bogie pitch motion, with phase difference between these two motion components and the converter vibration.

Considering the dominant wavelength in longitudinal level irregularity at 5.45m due to the slab track, four resonance speeds are obtained at 157 km/h, 173 km/h, 212 km/h and 230 km/h. Fig. 4 shows the power spectral density (PSD) of car-body acceleration over the front bogie and at body centre obtained processing the results of simulations performed at these speeds. In each PSD curve, a marked peak confirms the expected resonance condition. The magnitude of the PSD in resonance, at most speeds, is larger at car-body centre, due to the shape of the first car-body bending mode. This analysis shows that the vehicle is particularly sensitive to longitudinal level irregularities when travelling at speeds close to 230km/h. For this reason, the design of the LQG controller is initially focussed on this speed, while the effect of vehicle speed in the range 150-350 km/h is analysed later.

The analysis also shows that bogie bounce is not the only component of bogie motion having an impact on car-body bending vibration and instead the effect of bogie pitch on car-body bending is at least equally important and shall be considered in the design of the control strategy. As mentioned above, this is due to the strong coupling effect caused by the traction links and yaw dampers.

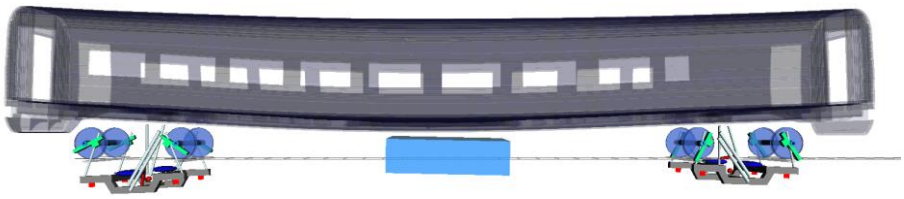

(a) Car-body bending coupled with bogie bounce at 8.0 Hz

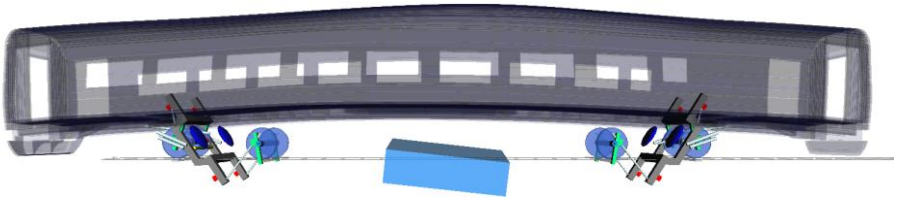

(b) Car-body bending coupled with bogie pitch and longitudinal motions at 8.8 Hz

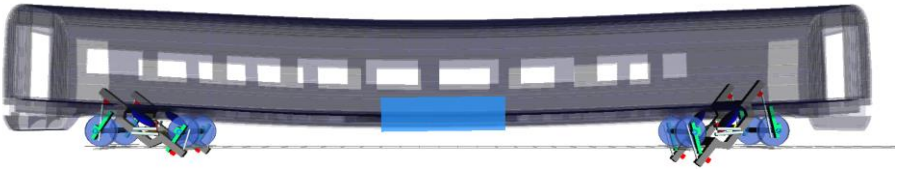

(c) Car-body bending coupled with bogie pitch motion at 10.9 Hz

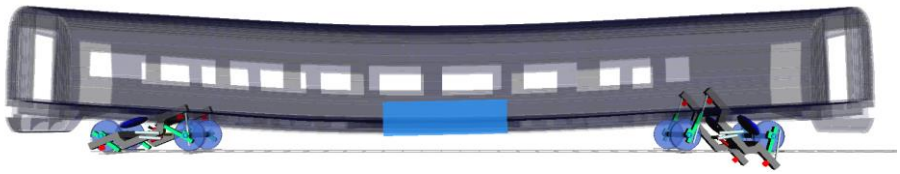

(d)Car-body bending coupled with bogie pitch motion (opposite direction) at 11.8 Hz
Fig. 3 Coupled mode shape between car-body bending and bogie vibrations

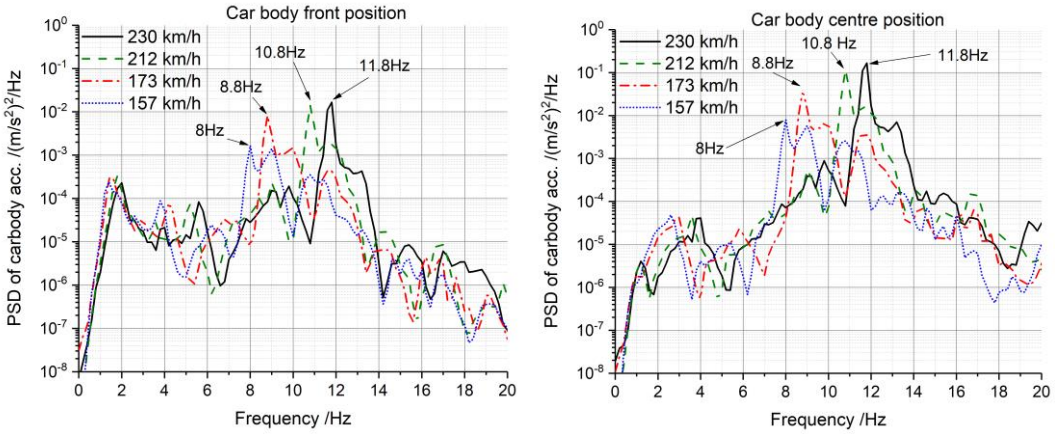

Fig. 4 PSDs of car-body vertical acceleration for the passive vehicle from the FMBS model, Left: car-body front, Right: car-body centre

3.1.2 Model of the semi-active dampers

To consider the case of a vehicle equipped with SAPS, semi-active dampers are considered in the FMBS model through co-simulation between SIMPACK and Simulink. The semi-active dampers are modelled as linear viscous dampers having a viscous damping coefficient that can be adjusted in a range from a minimum value d_{min} to a maximum value d_{max}. Additionally, the dynamics of the dampers is considered in the form of a 1-st order system causing a delay between the reference command and the force in the damper.

Given a reference control force $u_{ref,j}$ defined by the LQG controller (see Section 4) for the j^{th} semi-active damper, the ideal (i.e. with no delay) damping force $u_{d,j}$ in the same damper is defined based on the elongation speed of the damper $v_{P,j}$ as:

$$u_{d,j} = \begin{cases} d_{min} v_{P,j} & (u_{ref,j} \cdot v_{P,j} < 0) \\ sign(v_{P,j}) \cdot max\left[min(|d_{max} v_{P,j}|, |u_{ref,j}|), |d_{min} v_{P,j}|\right] & (u_{ref,j} \cdot v_{P,j} \geq 0) \end{cases} \quad (2)$$

In this work the minimum and maximum damping values are assumed to be 5kNs/m and 100kNs/m respectively, based on some laboratory tests performed at Politecnico di Milano on a prototype damper and also on the values reported in [19].

The actual force $u_{a,j}$ produced by the semi-active damper is then defined considering the

response time of the damper through a first-order low-pass filter:

$$\dot{u}_{a,j} = -\frac{u_{a,j}}{T_r} + \frac{u_{d,j}}{T_r} \tag{3}$$

MR Dampers are among the best suited damper technologies for SAPS, thanks to their short response time which makes them capable of satisfactory vibration control at frequencies above 10Hz [20,21].

The Magnetorheological fluid can react to the change of magnetic field in only a few milliseconds, so the response time of MR dampers is in the range 20ms to 30ms [22,23]. Therefore, the time constant T_r is set to 10 ms, corresponding to 30ms response time ($3T_r$). The LQG controller and the model of the semi-active dampers are defined in Simulink, and the actual damping forces $u_{a,j}$ from all semi-active dampers are fed to the FMBS SIMPACK model through co-simulation.

3.2 Simplified 7-DOF vehicle model

3.2.1 Introduction of 7-DOF-Coupling model

The analysis of car-body-to-bogie coupling in Sections 2 and 3.1.1 shows that the classic simplified 7-DOF model in Fig. 1 is not fully suited for the design of a control strategy for car-body vibration, as it misses the coupling between car-body bending and bogie pitch motions, which is a crucial feature for a real HS vehicle. A first attempt to define a more suitable simplified model is presented in reference [17], where a 12-DOF model is proposed. This 12-DOF model shows a good matching to the more detailed FMBS models, but it is somehow too complex for the design of a model-based controller, which should be kept as simple as possible to ensure a fast calculation in real-time. In this paper, a new simplified model named 7-DOF-Coupling vehicle model is established, which is simpler than the 12-DOF model, but retains the capability to describe properly the coupling between car-body bending and bogie motion. s

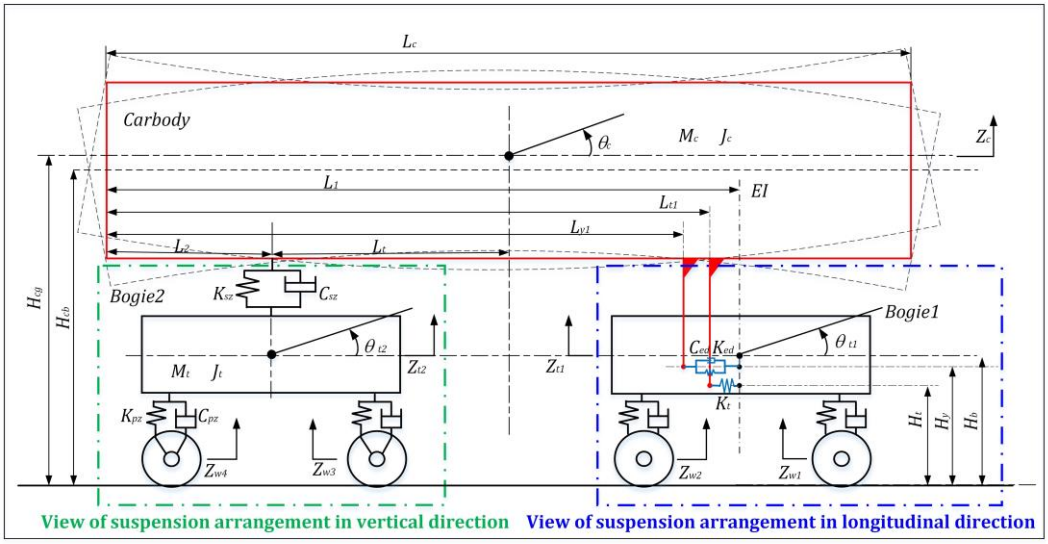

Fig. 5. 7-DOF-Coupling vehicle model

The 7-DOF-Coupling model is shown in Fig. 5: the arrangement of the vertical suspension is displayed on the left bogie and the arrangement of the longitudinal suspension is shown on the right bogie. The proposed model has the same DOFs as the classic 7-DOF model, i.e. car-body bounce (Z_c), pitch (θ_c) and first bending (q) mode, and bogie bounce (Z_{t1}, Z_{t2}) and pitch (θ_{t1}, θ_{t2}). The mass of the converter is incorporated in the inertia of the car-body. The model of the vertical secondary suspension considers a linear spring and viscous dashpot in vertical direction, like the classic model, but additionally includes longitudinal springs and dashpots connecting the car-body to the bodies, to model the effect of the traction links and yaw dampers. Yaw dampers are often modelled according to a Maxwell model (dashpot C_d with serial stiffness K_d), which is here replaced by an equivalent Kelvin–Voigt model (spring and dashpot in parallel) to avoid the need to introduce the internal states required by the Maxwell model. The parameters of the Kelvin-Voigt model, C_{ed} and K_{ed}, are derived from those of the Maxwell model using the relationships in Eq. (4), where f is frequency [24], . This equation shows that the equivalent stiffness and damping of the Kelvin–Voigt are frequency-dependent, however with the aim of simplifying the model, constant values are set for these parameters, setting frequency f to the value corresponding to the resonance of the modes in Fig. 3 involving the coupling of car-body bending and bogie pitch.

$$\begin{cases} C_{ed} = \frac{C_d {K_d}^2}{{K_d}^2 + {C_d}^2 f^2} \\ K_{ed} = \frac{K_d {C_d}^2 f^2}{{K_d}^2 + {C_d}^2 f^2} \end{cases} \tag{4}$$

Traction links are modelled using a linear spring with stiffness K_t. The bogie longitudinal motions are not considered, since the coupling between car-body bending and bogie pitch

is sufficient to reproduce the modes of the FMBS model found in the frequency range of interest. The parameters of the 7-DOF-Coupling model are summarized in Table A.1.

3.2.2 Simplified model of the flexible car-body

The car-body first bending vibration is represented using an Euler beam model, see Eq. (5).

$$w(x,t) = Y(x)q(t) \tag{5}$$

where, $w(x,t)$ expresses the displacement of the beam at position *x*, time *t*; $Y(x)$ describes the shape of the first bending mode, unchanging with time, see Eq. (6),

$$Y(x) = (cos\,\beta_1 x + cosh\,\beta_1 x) - \frac{cos\,\beta_1 L_c - cosh\,\beta_1 L_c}{sin\,\beta_1 L_c - sinh\,\beta_1 L_c}(sin\,\beta_1 x + sinh\,\beta_1 x) \tag{6}$$

where $\beta_1 L_c = 4.7300$ [25].

In Eq. (5), $q(t)$ describes a time-dependent scaling coefficient applied to the shape $Y(x)$ of the bending mode. The dynamics of this modal coordinate is governed by Eq. (7):

$$\ddot{q} + 2\xi_1\omega_1\dot{q} + {\omega_1}^2 q = \frac{1}{M_c}\left\{\sum_{i=1,2}\left[F_{sz,i}Y(L_i) + F_{sxt,i}d_{cbt}Y'(L_{ti}) + F_{sxy,i}d_{cby}Y'(L_{ti})\right]\right\} \tag{7}$$

where, $\omega_1 = 2\pi f$ expresses the natural angular frequency of the bending mode; ξ_1 is the non-dimensional damping ratio. $F_{sz,i}$, $F_{sxt,i}$, and $F_{sxy,i}$ *(i=1,2)* respectively refer to vertical force from air springs, and two longitudinal forces from the traction links and yaw dampers. d_{cbt} and d_{cby} are distances from the height of the car-body bending neutral axis (H_{cb}) to the height of the traction links (H_t) and yaw dampers (H_y), i.e. $d_{cbt} = H_{cb} - H_t$; d_{cby}=$H_{cb} - H_y$.

Although the use of the Euler beam model to consider the effect of car-body bending flexibility is common in the literature, see [3,9,14,16], there is a significant deviation between the actual shape of the first bending mode and the one provided by the simplified beam model, because the real car-body behaves structurally as a shell with variable properties along the longitudinal axle, and this complex structural behaviour is only partly captured by the Euler beam model. To improve the correspondence of the simplified model to the actual behaviour of the car-body, a calibration of the beam model is performed with the reference to the FE car-body model.

In the calibration, the six DOFs related to the rigid motion of the car-body in the FMBS model are constrained, obtaining a model that only considers car-body first bending vibration based on the modal synthesis in SIMPACK. Two equal, in-phase vertical forces are applied at the positions where the car-body sits over the air-springs, shown by the yellow arrows in Fig. 6 (a) and two longitudinal forces, having the same amplitude but

opposite phase are applied at the yaw dampers mount points, see the red arrows. Both vertical and longitudinal forces are generated as white noise, then processed by a low-pass filter with cut-off frequency 20 Hz. The time histories of applied force are shown in Fig. 6 (b).

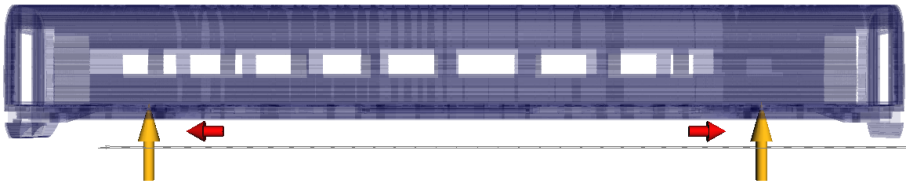

(a) FE car-body model in load condition

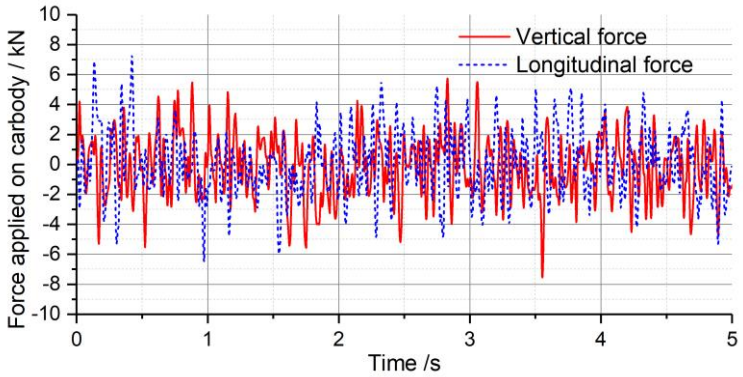

(b) Time history of applied forces

Fig. 6 The calibration of the beam model

The car-body vertical acceleration measured at the centre and two positions above the bogie centres are used as the indicators to calibrate the damping ratio and, from the comparison of the two models, the value $\xi_1 = 3\%$ is found to provide the best match. As an example, Fig. 7(a) compares the vertical acceleration at car-body centre for the SIMPACK flexible model and for the simplified Euler beam model, showing satisfactory agreement.

The height of the beam's neutral axis H_{cb} is the other parameter which is identified from the comparison of the two sets of results, considering in this case as the indicators the longitudinal acceleration at the mount points of these components, based on Eq. (1). The value $H_{cb} = 1.6m$ is found, from which the vertical distances from the neutral axis to the yaw damper and traction link mounts d_{cby} and d_{cbt} are obtained. Fig. 7(b) compares the longitudinal acceleration of the yaw damper mount point for the two models, after the calibration of the simplified one.

Despite the calibrated beam model still involves significant approximation in describing the flexible motion of the car-body, it provides a sufficiently good estimate of the car-body vertical acceleration at the three positions considered by the LQG controller (see Section 4) in regard to the vertical ride comfort evaluation, and a good estimate for the longitudinal motion at the damper and traction link mounts, so as to reproduce correctly the coupling

between car-body bending and bogie pitch due to the traction links and yaw dampers, which is pivotal to the development of the model-based controller.

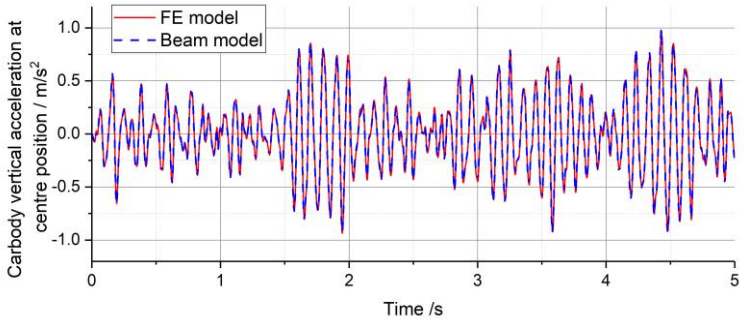

(a) Car-body vertical acceleration at bogie centre

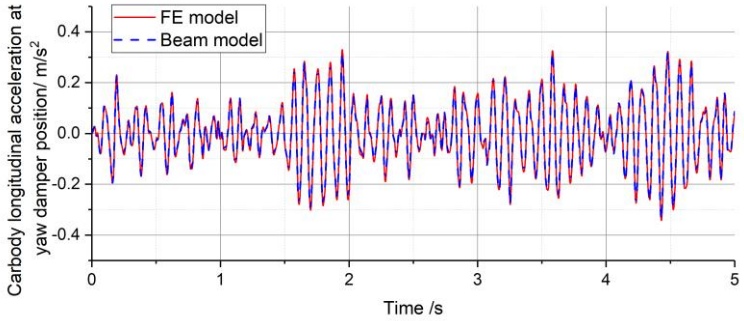

(b) Car-body longitudinal acceleration where yaw damper is installed

Fig. 7 Comparison of car-body acceleration of the FE model and of the simplified beam model after beam model calibration

3.2.3 Equations of motion of the 7-DOF model

The set of equations of motion for the 7-DOF coupling model are summarised in Eq. (8). The expressions of the vertical forces in the secondary suspension, $F_{sz,i}$ (1=1,2) and in the primary suspensions, $F_{pz,i}$ (i=1,…,4) are provided by Eq. (9), where d_{by} and d_{bt} refer to the distances from the height of bogie centre of gravity to the height of yaw dampers and traction links; and similarly, d_{cgy} and d_{cgt} are distances from the height of car-body centre of gravity to yaw dampers and traction links.

$$\begin{cases} \mathrm{M_c}\ddot{\mathrm{Z}}_\mathrm{c} = \mathrm{F_{sz,1}} + \mathrm{F_{sz,2}} \\ J_c\ddot{\theta}_c = L_tF_{sz,1} - L_tF_{sz,2} + D_{cgy}\left(F_{sxy,1} + F_{sxy,2}\right) + D_{cgt}\left(F_{sxt,1} + F_{sxt,2}\right) \\ M_t\ddot{Z}_{t1} = -F_{sz,1} + F_{pz,1} + F_{pz,2} \\ J_t\ddot{\theta}_{t1} = L_w(F_{pz,1} - F_{pz,2}) - d_{by}F_{sxy,1} - d_{bt}F_{sxt,1} \\ M_t\ddot{Z}_{t2} = -F_{sz,2} + F_{pz,3} + F_{pz,4} \\ J_t\ddot{\theta}_{t2} = L_w(F_{pz,3} - F_{pz,4}) - d_{by}F_{sxy,2} - d_{bt}F_{sxt,2} \\ \ddot{q} + 2\xi_1\omega_1\dot{q} + {\omega_1}^2 q = \frac{1}{M_c}\left\{\sum_{i=1,2}\left[F_{sz,i}Y(L_i) + F_{sxt,i}d_{cbt}Y'(L_{ti}) + F_{sxy,i}d_{cby}Y'(L_{ti})\right]\right\} \end{cases} \tag{8}$$

$$
\begin{cases}
F_{sz,1} = C_{sz}[\dot{Z}_{t1} - (\dot{Z}_c + L_t\dot{\theta}_c + Y(L_1)\dot{q}] + K_{sz}[Z_{t1} - (Z_c + L_t\theta_c + Y(L_1)q)] \\
F_{sz,2} = C_{sz}[\dot{Z}_{t2} - (\dot{Z}_c - L_t\dot{\theta}_c + Y(L_2)\dot{q})] + K_{sz}[Z_{t1} - (Z_c - L_t\theta_c + Y(L_2)q)] \\
F_{sxt,1} = K_{sx}\left[\theta_{t1}d_{bt} - (\theta_c d_{cgt} + Y'(L_{t1})qd_{cbt})\right] \\
F_{sxt,2} = K_{sx}\left[\theta_{t2}d_{bt} - (\theta_c d_{cgt} + Y'(L_{t2})qd_{cbt})\right] \\
F_{sxy,1} = C_{ed}\left[\dot{\theta}_{t1}d_{by} - (\dot{\theta}_c d_{cgy} + Y'(L_{y1})\dot{q}d_{cby})\right] + K_{ed}\left[\theta_{t1}d_{by} - (\theta_c d_{cgy} + Y'(L_{y1})qd_{cby})\right] \\
F_{sxy,2} = C_{ed}\left[\dot{\theta}_{t2}d_{by} - (\dot{\theta}_c d_{cgy} + Y'(L_{y2})\dot{q}d_{cby})\right] + K_{ed}\left[\theta_{t2}d_{by} - (\theta_c d_{cgy} + Y'(L_{y2})qd_{cby})\right] \\
F_{pz,1} = C_{pz}[\dot{Z}_{w1} - (\dot{Z}_{t1} + L_w\dot{\theta}_{t1})] + K_{pz}[Z_{w1} - (Z_{t1} + L_w\theta_{t1})] + u_{a1} \\
F_{pz,2} = C_{pz}[\dot{Z}_{w2} - (\dot{Z}_{t1} - L_w\dot{\theta}_{t1})] + K_{pz}[Z_{w2} - (Z_{t1} - L_w\theta_{t1})] + u_{a2} \\
F_{pz,3} = C_{pz}[\dot{Z}_{w3} - (\dot{Z}_{t2} + L_w\dot{\theta}_{t2})] + K_{pz}[Z_{w3} - (Z_{t2} + L_w\theta_{t2})] + u_{a3} \\
F_{pz,4} = C_{pz}[\dot{Z}_{w4} - (\dot{Z}_{t2} - L_w\dot{\theta}_{t2})] + K_{pz}[Z_{w4} - (Z_{t2} - L_w\theta_{t2})] + u_{a4}
\end{cases} \quad (9)
$$

The wheelset vertical displacements and velocities $Z_{w\mathrm{i}}$ and $\dot{Z}_{wi}$ (i=1, …,4) are derived from a measured profile of track irregularity, in the form of a spatial profile which is then translated in a time series based on the speed and distance between axles. The vehicle in passive mode has no control force and thus the components u_{ai} for primary vertical forces $F_{pz,i}$ (i=1,…,4) is zero. When SAPS is equipped in the vehicle, the damping C_{pz} becomes zero and the control forces u_{ai} are adopted. To get the applied control force u_{ai}, the reference control force u_{ref} is firstly computed from the LQR controller (see Eq. (16) in Section 4) and then it is processed using Eq. (2) and (3) to consider the dynamics of the semi-active damper.

It is worth mentioning that the equations of the classic 7-DOF model shown in Fig. 1 can be easily derived from Eq. (8) and (9), just nulling the stiffness and damping parameters of the yaw dampers and traction links.

Fig. 8 compares the results obtained using the FMBS model and the two simplified models in terms of the PSDs of car-body accelerations at front and centre positions, for the passive vehicle running at 230 km/h. A good agreement among the three models can be found in the frequency range below 8Hz, both at car-body front and at centre positions. However, a remarkable difference is found at higher frequencies and, in particular, the classic 7-DOF model misses completely to reproduce the large peak of the PSD at 11.8 Hz. The 7-DOF-Coupling model instead shows satisfactory agreement to the FMBS model in the entire frequency range up to 20 Hz, particularly in terms of the peak at 11.8 Hz which has a main effect on ride quality.

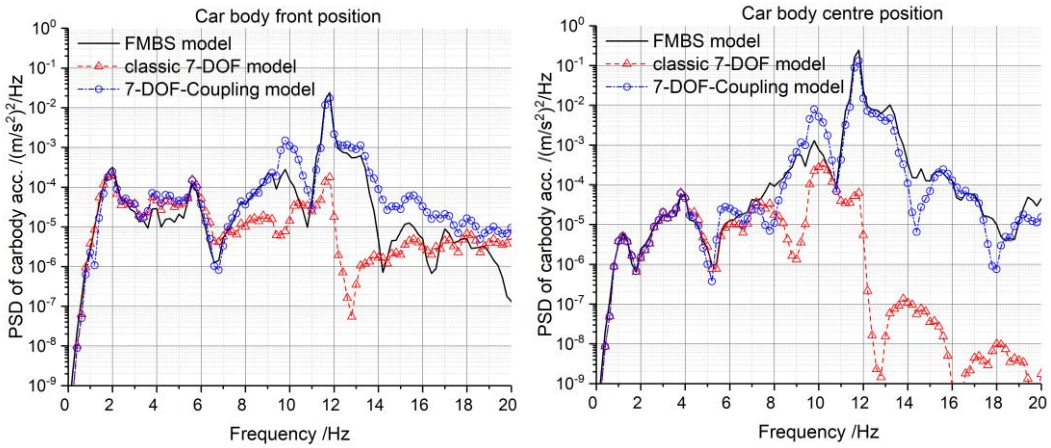

Fig. 8 PSD of car-body acceleration for the passive vehicle: comparison of the FMBS and 7-DOF-Coupling models, Left: car-body front, Right: car-body centre

4 Design of the LQG controller for the SAPS

The Linear Quadratic Gaussian (LQG) is a classic model-based controller, consisting of a Linear Quadratic Regulator (LQR) to calculate the feedback control force, and a Kalman filter (KF) for state estimation. It provides optimal control for the system through full-state feedback. The gain matrix defining state feedback is obtained through the minimisation of a cost function J, in which the control targets are defined in the linear-quadratic form. A detailed explanation for the working principle of LQG can be found in [26].

For the development of the LQG controller for the SAPS, the differential equations for the 7-DOF-Coupling model, defined in Section 3 are expressed as state-space equations, as shown below:

$$\dot{X} = AX + BU + GW \tag{10}$$

where X represents the state variables considered in the vehicle model, see Eq. (11); A, B and G are constant-valued matrices allowing to represent the set of differential equations (8) and (9) in state-space form.

$$X = [Z_c \quad \dot{Z}_C \quad \theta_c \quad \dot{\theta}_c \quad Z_{t1} \quad \dot{Z}_{t1} \quad \theta_{t1} \quad \dot{\theta}_{t1} \quad Z_{t2} \quad \dot{Z}_{t2} \quad \theta_{t2} \quad \dot{\theta}_{t2} \quad q \quad \dot{q}] \tag{11}$$

U contains the controllable damping force, see Eq. (12)

$$U = [u_{a1}, u_{a2}, u_{a3}, u_{a4}]^T \tag{12}$$

W refers to the excitation from wheelsets due to the track irregularity, see Eq. (13)

$$W = [\dot{Z}_{w1}, \dot{Z}_{w2}, \dot{Z}_{w3}, \dot{Z}_{w4}, Z_{w1}, Z_{w2}, Z_{w3}, Z_{w4}]^T \tag{13}$$

A 7-sensor measuring scheme is adopted, which was also considered in [14,16], see Fig. 9. The blue circles with labels "S_j" (j=1, … ,7) illustrate the positions of accelerometers, three on the car-body floor and four mounted at the front and rear positions of the bogie.

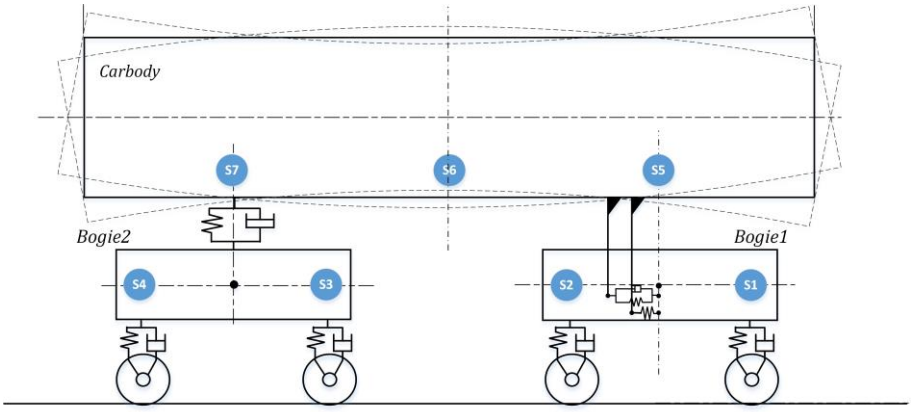

Fig. 9. 7-Location of sensors for LQG control.

The seven measured accelerations are collected in the observation vector Y_s, defined according to Eq. (14), where C_s, D_s and H_s can be derived according to seven accelerations as superpositions of different vibration modes, and V represents the measuring noise.

$$Y_s = C_s X + D_s U + H_s W + V \tag{14}$$

The measured seven accelerations are fed to the Kalman filter, where the information of the vehicle model and measurements will be synthesized to estimate the full state variables $\hat{X}$. In the design of the Kalman filter, the covariance of system disturbance W and measuring noise V are configured, based on the extent to which the model and the measured quantities can be trusted. Then, the observer gain matrix K_f can be obtained by solving an optimization problem to minimize the errors between the real X and estimated $\hat{X}$. Once the K_f is obtained, the estimated variables are computed according to Eq. (15).

$$\dot{\hat{\mathrm{X}}} = \left(A - K_f C_s\right)\hat{\mathrm{X}} + \left(B - K_f D_s\right)U + K_f Y_s \tag{15}$$

Afterwards, the estimated full-state variables are multiplied by a feedback control gain matrix K_{LQR} to get the reference control force U_{ref}, see Eq. (16).

$$U_{ref} = -K_{LQR}\hat{X} \tag{16}$$

It should be noted that the simplified model is two-dimensional, with no consideration of the lateral dimension. Thus, the four scalar components of vector U_{ref} represent the sum of the two forces applied by the two semi-active dampers mounted at the two sides of a same wheelset. The reference force for each damper is therefore obtained considering an equal share of the control force on the two sides.

The control gain K_{LQR} in Eq. (16) is obtained by solving a Riccati equation to minimize the cost function J_{LQR}, defined in Eq. (17),

$$J_{LQR} = \lim_{t\to\infty} \frac{1}{t} \int_0^t (Y_t{}^T Q Y_t + U^T R U)\, dt \tag{17}$$

where the vectors U and Y_t contain the control forces and vibration quantities to be minimized.

In order to control each vehicle vibration mode separately, Y_t is defined consisting of car-body bounce, pitch and bending accelerations, and bogie bounce and pitch velocities, see Eq. (18)

$$Y_t = [\ddot{Z}_c, L_t\ddot{\theta}_c, \ddot{q}_1, \dot{Z}_{t1}, \dot{Z}_{t2}, L_w\dot{\theta}_{t1}, L_w\dot{\theta}_{t1}]^T \tag{18}$$

The Q and R are diagonal matrixes defining the weights between vibration modes and control forces, see Eq. (19)

$$\begin{cases} Q = Diag(W_{cz}, W_{c\theta}, W_q, W_{tz}, W_{tz}, W_{t\theta}, W_{t\theta}) \\ R = Diag(W_f, W_f, W_f, W_f) \end{cases} \tag{19}$$

Since all dampers in the vehicle have the same characteristics, the same value W_f is used in all rows of the matrix R defining the weight of the control force. In matrix Q, instead, different scalar weights are introduced in each row, to reflect the fact that each mode of vibration affects in a different way the dynamics of the vehicle, and also to consider that the observed variables in vector Y_t are not dimensionally homogeneous.

To derive suitable values of the weights in matrices Q, several simulations are performed starting with one-at-time control of each observed variable. In this way, starting values are found for weights $W_{cz}, W_{c\theta}, W_q, W_{tz}, W_{tz}, W_{t\theta}, W_{t\theta}$ which are then used to define two different multi-mode versions of the LQG controller, see Section 5 for more details. It is worth noting that the value of the single gain coefficient W_f defining matrix R only affects the scaling of the terms in matrix Q. Hence, a fixed value of matrix R is maintained for all versions of the LQG controller. ~~In Section 5, we apply a fixed value for R and different settings for Q to realise the tuning between control effect and suitable control force with different control targets.~~

Considering the two simplified models introduced in Section 3.2. The LQG controller can be built based on the classic 7-DOF model, or the new 7-DOF-Coupling model. The comparison of the two model-based LQG controllers is analysed in Section 5.3.

5 Performance of the SAPS with LQG controller

The performance of the SAPS system is assessed by means of numerical simulations performed using the SIMPACK FMBS model of the vehicle introduced in section 3.1 in co-simulation with a model of the controller and of the semi-active dampers implemented in Simulink. The analysis is firstly focussed on the speed of 230 km/h which, as discussed above, is particularly meaningful. Then, the analysis is extended to the entire range of speed

150-350 km/h and finally, the impact of using the modified 7-DOF model instead of the classic one in the design of the LQG controller is assessed.

5.1 Performance of SAPS at speed 230km/h

A first assessment of the performance of the semi-active suspensions focusses on the resonance speed 230 km/h, which is the most critical speed in terms of ride quality, based on the analysis reported in Section 3.1.1.

Different versions of the LQG controller are considered. In a first stage, the different components of vehicle motion represented by the scalar elements in vector Y_t are controlled one-at-a-time by setting a non-zero weight in just one term of the diagonal matrix Q, see Eq. 19. Different values of the non-zero term in matrix Q are considered, but for the sake of brevity only the one providing sufficiently good result in terms of reducing car-body vibration is considered below. The R weight matrix defining the effect of control forces on the cost function is set to $R = \mathrm{Diag}(10^{-4}, 10^{-4}, 10^{-4}, 10^{-4})$. This value of the R matrix is kept unchanged in all analyses reported below.

Fig. 10 compares the PSD curves of acceleration at car-body front and centre positions for the passive vehicle and for the vehicle with SAPS, considering one-at-a-time LQG configuration. Controlling only car-body bounce with $W_{cz}= 1 \times 10^7$, (i.e. defining $Q = Diag(1 \times 10^7, 0,0,0,0,0,0)$) results in reduced vibration at car-body centre in the low frequency range, but causes an increase of vibration at higher frequencies, see the blue dash line in Fig. 10(a). Similarly, controlling only car-body pitch with $W_{c\theta}=1 \times 10^6$ provides a small benefit for rigid vibration at car-body front, but again leads to larger vibration at higher frequencies, as shown the green dash-dot line in Fig. 10(a). Different from the two car-body rigid modes control, the one-at-a-time control of car-body bending, represented using red dot line, provides a significant reduction of vibration at 11.8Hz, corresponding to the resonance of the car-body excited by track irregularities when the vehicle runs at 230 km/h, despite a slight increase of vibration is observed in the low frequency range. It is important to underline that the use of the 7-DOF Coupling model is essential to the success of the LQG controller in this case, and that using the classic 7-DOF model instead would result in decreased ride quality compared to the passive vehicle, as will be shown in Section 5.3.

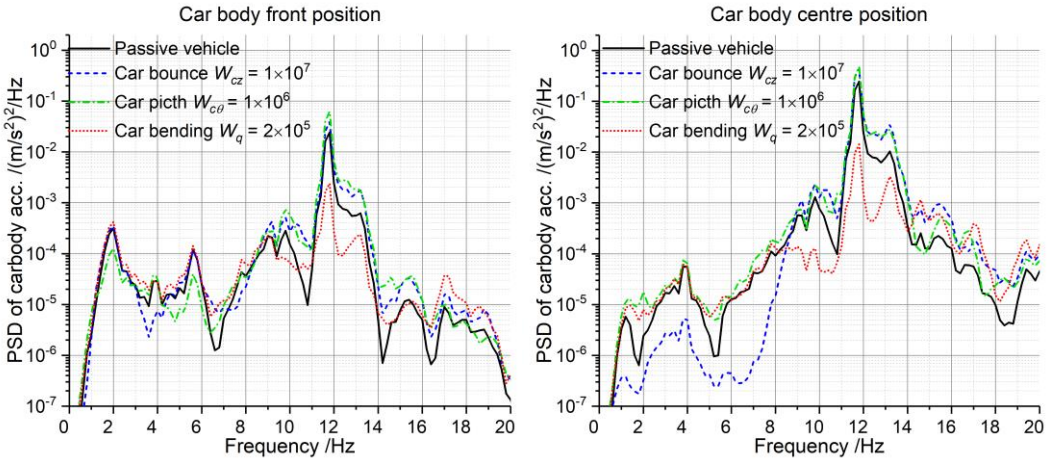

(a) three car-body mode controls, Left: car-body front, Right: car-body centre

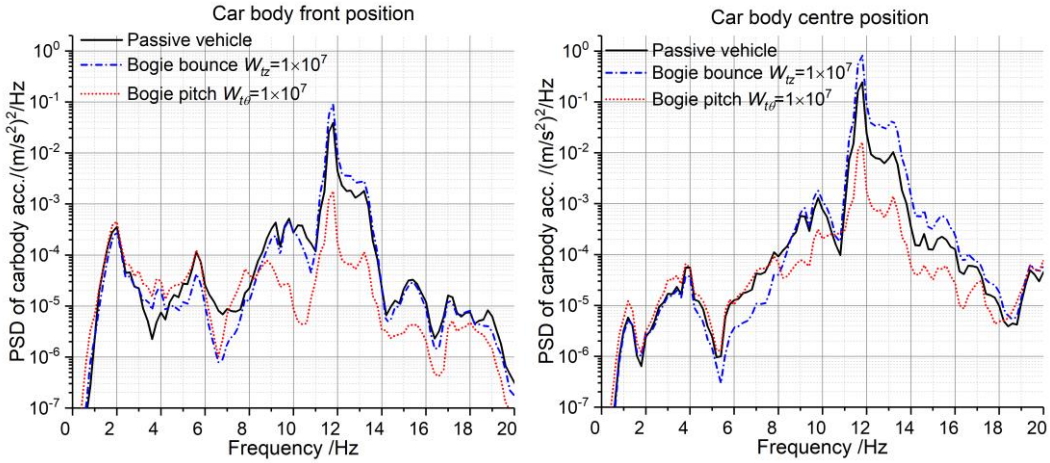

(b) two bogie mode controls, Left: car-body front, Right: car-body centre

Fig. 10 PSD of car-body acc. with one-at-time configurations of the LQG controller

In Fig. 10 (b), the one-at-a-time control of bogie bounce provides results similar to those obtained for car-body bounce and car-body pitch control, i.e. a slight benefit in the low-frequency range which comes at the expense of significant increase of vibration at higher frequencies. Finally, the one-at-a-time control of bogie pitch provides a very significant benefit in the high-frequency range, and a reduction of car-body vibration is comparable to the control of car-body bending. This last result may seem contradictory, as a large benefit is obtained in the high-frequency range by controlling a rigid mode of the vehicle, but can be explained in the light of the strong coupling between car-body bending and bogie pitch. This also shows that a control strategy aimed at mitigating bogie pitch can be highly effective in improving ride quality, suggesting that simpler control strategies such as modal sky-hook damping applied to bogie pitch could be successfully applied.

Both controllers on car-body bending and bogie pitch effectively mitigate car-body bending vibration, but controlling the bending is less effective with mitigating car-body vibration at frequencies beyond 15 Hz, which is probably due to the effect of modelling errors in the

simplified model of car-body flexibility.

To quantify the separate control effects for rigid and flexible vibrations under the above-mentioned control configurations, the root mean square (RMS) value of car-body acceleration evaluated in the centre and over the two bogies, are analysed using two band-pass filters with passband 1-8Hz and 8-16Hz respectively, given the specific resonances of the considered HS vehicle.

Table 1 reports the variation of the band-limited RMS values, using the passive vehicle as a reference. For rigid vibration ranging from 1Hz to 8Hz, the two car-body rigid mode controls (W_{cz} *and* $W_{c\theta}$) are less effective than the bogie bounce control (W_{tz}) at all the considered measuring locations, and the car-body pitch leads to slightly increased RMS at car centre because the control benefits from car-body rigid modes at a frequency are cancelled out by the degradation at other frequencies. In the frequency range 8-16Hz, the band-limited RMS of structural vibration is remarkably reduced by 71% and by 72% at car-body centre, respectively using car-body bending and bogie pitch control configurations, which confirms the above analysis based on the PSD curves.

Table 1. Variation of the band-limited RMS of car-body acceleration using SAPS with LQG control (speed 230km/h)

	RMS of rigid vibrations (1-8Hz)							RMS of flexible mode vibrations (8-16Hz)						
	One-at-a-time					Multimode		One-at-a-time					Multimode	
	W_{cz}	$W_{c\theta}$	W_q	W_{tz}	$W_{t\theta}$	Q_1	Q_2	W_{cz}	$W_{c\theta}$	W_q	W_{tz}	$W_{t\theta}$	Q_1	Q_2
Car front	1%	-25%	18%	-16%	19%	-29%	-36%	30%	61%	-65%	92%	-71%	-74%	-82%
Car centre	-71%	32%	13%	-32%	7%	-65%	-59%	39%	43%	-71%	86%	-72%	-78%	-80%
Car rear	0%	-24%	13%	-17%	19%	-35%	-38%	24%	35%	-37%	79%	-69%	-72%	-79%

To fully exploit multi-mode control of vibration, two other configurations of the LQG controller are also considered, with weights of the Q matrix defined by Eq. (20).

$$\begin{cases} Q_1 = Diag(1\times10^7, 1\times10^6, 2\times10^5, 0,0,0,0) \\ Q_2 = Diag(1\times10^7, 1\times10^6, 2\times10^5, 1\times10^7, 1\times10^7, 1\times10^7, 1\times10^7) \end{cases} \quad (20)$$

Configuration Q_1 aims at controlling all three car-body modes using suitable weight numbers suggested by the previous one-at-a-time analyses. Configuration Q_2 makes use of the same weights as configuration Q_1 for car-body modes and additionally includes non-zero weights for bogie modes. The results for these two configurations in terms of reduction of the banded RMS are also included in Table 1, and the PSD curves of acceleration at car-body front and centre are shown in Fig. 11. Both configurations can remarkably reduce the

vibration with respect to the passive vehicle in the entire 1-20 Hz frequency range, so that a further improvement with respect to the one-at-time control strategies can be obtained. The configuration Q_2 provides a slightly larger vibration reduction than Q_1 in the 8-16Hz frequency range. Figure 12 also presents the comparison of car-body acceleration measured at centre position in time domain, clearly exhibiting the reduction of acceleration magnitude by a factor more than 2 when the proposed LQG controllers are applied. Accelerations are shown over a short time window to improve the readability of the plot. Anyway, both Q_1 and Q_2 configurations provide fully satisfactory results, showing a reduction of the vertical ride index N_{mvz} [27] by 68% and 75% at car front and 74% and 76% at car centre, compared to the passive vehicle.

Besides vehicle vibration, the damping force of the MR damper is also examined, as shown in Figure 13. The maximum amplitude of the damping force for the two configurations of the LQG controller is under 5kN, which is easily achievable for a normal MR damper. The frequency analysis of the damping force shows that the dominating working frequency of the damper is in line with the most critical resonance vibration at nearly 12Hz.

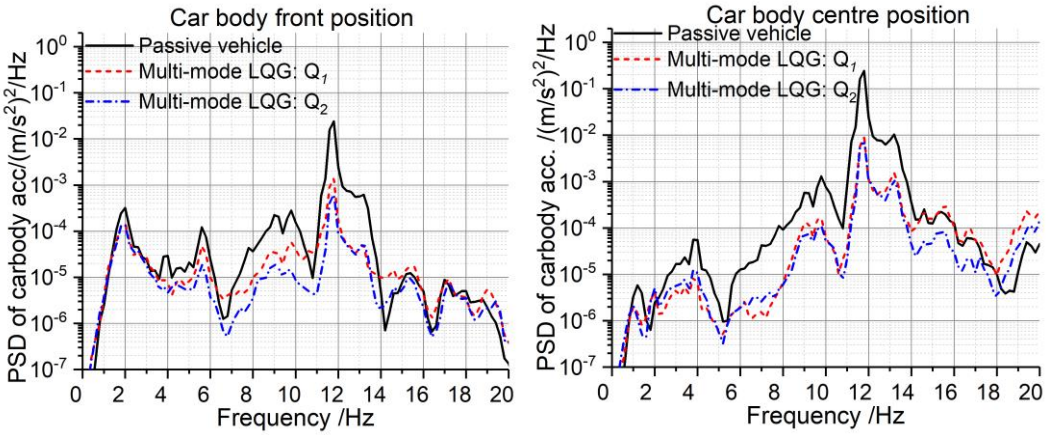

Fig. 11 PSD of car-body acc. with multi-mode configurations of the LQG controller. Left: car-body front, Right: car-body centre

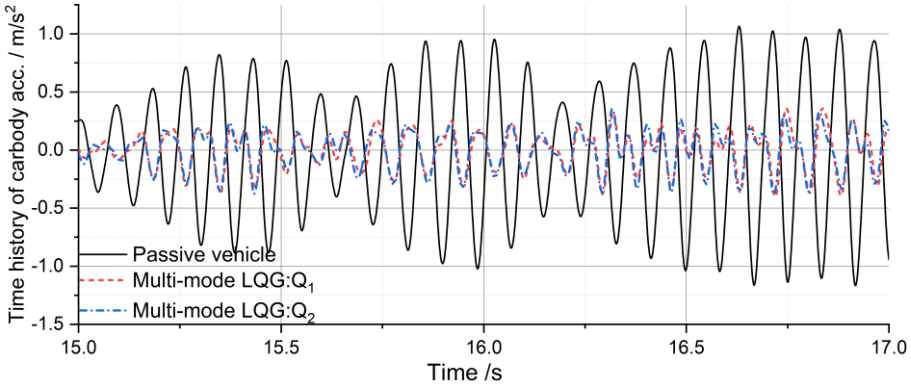

Fig. 12 Time histories of car-body acceleration at car centre for the passive vehicle and for the

active vehicle considering two configurations of the LQG controller

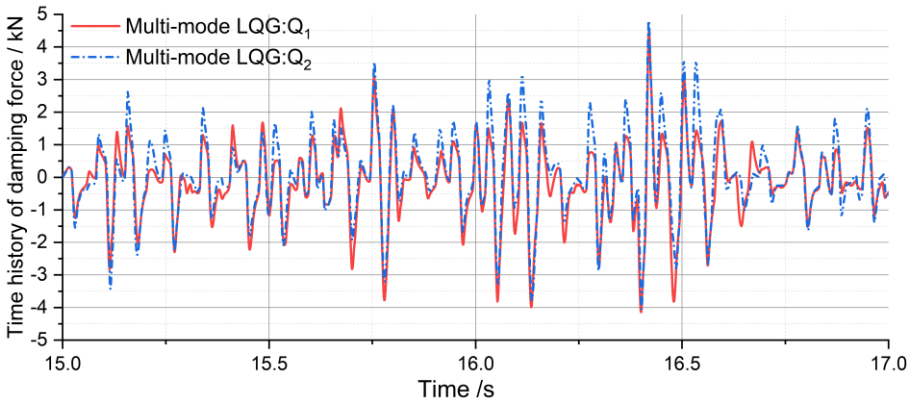

Fig. 13 Time histories of damping force for two configurations of the LQG controller

5.2 Performance of SAPS at different speed levels.

The simulations in Section 5.1 are performed at speed 230km/h where the passive vehicle is known to have the worst situation of ride comfort due to the resonance of car-body bending vibration. However, the analysis of the passive vehicle provided in Section 3.1.1 shows that there are other resonance speeds that may affect negatively ride quality. Thus, it is necessary to extend the analysis to confirm if the LQG controller is able to mitigate effectively car-body vibration in the entire range of speed of interest. Particularly interesting in this regard is the behaviour of the controller at speed 157 km/h, because this speed corresponds to a resonance of the mode at 8.0 Hz in which car-body bending is coupled to bogie bounce instead of bogie pitch.

Fig. 14 compares the PSD curves of car-body acceleration (front and centre) for two one-at-time configurations, addressing bogie bounce and bogie pitch. At the resonance speed 157 km/h, bogie bounce control provides significant reduction of car-body bending vibration in the 8-12Hz range. By contrast, bogie pitch control is clearly less effective to attenuate flexible vibration than at speed 230km/h. It is concluded that the control effects of bogie bounce and pitch control are affected by the specific coupling taking place between car-body and bogie motion for the mode excited in resonance.

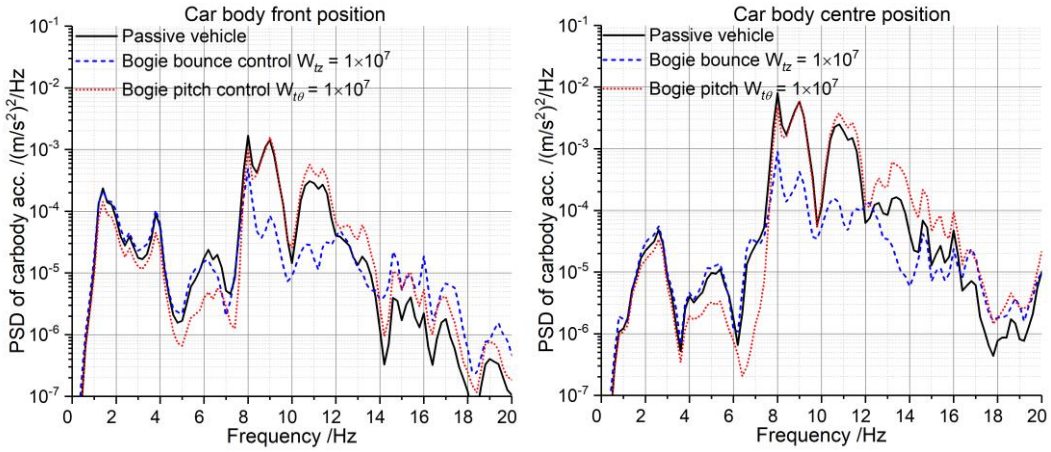

Fig. 14 PSD of car-body acceleration with selected one-at-a-time configurations of the LQG controller, Left: car-body front, right: car-body centre

Finally, the two multi-mode LQG configurations are applied at different speeds ranging from 150 km/h to 350 km/h, and the vertical ride index N_{mvz} is used to evaluate the improvement of ride comfort with SAPS. The ride indexes obtained at front and centre are normalized respectively using the maximum value at 230km/h as the reference. As shown in Fig. 15, the ride index does not increase monotonically with the speed and is instead strongly affected by different resonance effects involving car-body and bogie vibration. The implementation of SAPS, either using multi-mode Q_2 or Q_1 not only improves the ride comfort at the four particular speeds corresponding to the resonance as shown in Fig. 3 and Fig.4, but also at all other speeds. The performance of LQG in configuration Q_2 is more steadily effective than Q_1 at all speed levels, especially for those scenarios where a larger deviation between the simplified model and the FMBS model is expected.

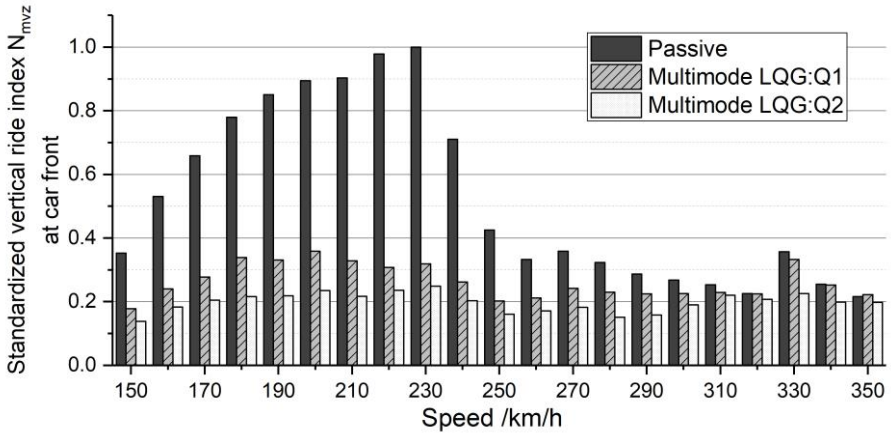

(a) Car front

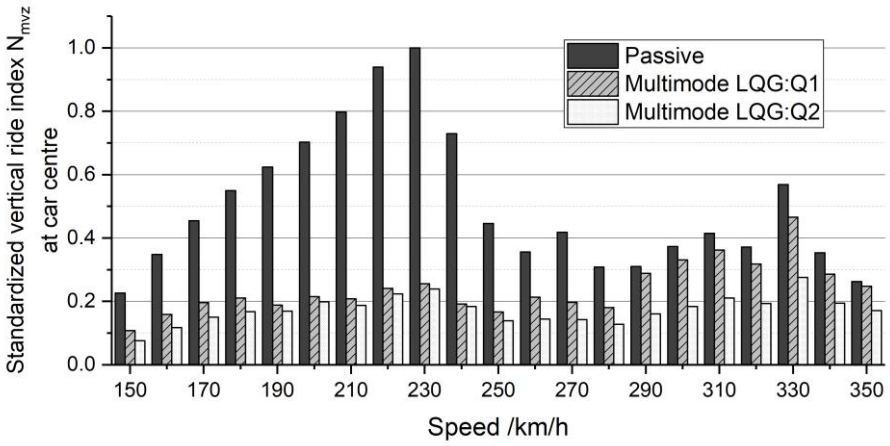

(b) car centre

Fig. 15 Values of the N_{mvz} ride quality index at different speed levels for the two multi-mode configurations of the LQG controller

The advantage of involving bogie motion together with car-body vibration in the design of the controller, as done with the Q_2 configuration, can be understood from the viewpoint of control robustness. It is recalled that the parameters of the simplified model are derived for the FMBS vehicle model featured at speed 230km/h, and these parameters may not be equally suited for the vehicle at other speed levels. For instance, the equivalent damping C_{ed} and stiffness K_{ed} for the Maxwell damper model are frequency-dependent (see Eq. 4), but this is not considered in the design of the controller. Therefore, a larger deviation between the simplified and the FMBS models is expected at other speeds. However, this error has a limited influence on the estimation of bogie motion components, whilst it is more significant for car body motion. This explains the superiority of configuration Q_2 over Q_1.

It is worth noting, in these simulations, the gain matrixes of the controller, i.e. the Q and R are kept fixed to a set of single value not depending on vehicle speed. Applying a gain scheduling approach through the design of specific LQG controllers at different speeds would further improve ride quality, but a speed-dependent controller would also increase the complexity of the system, which is beyond the research scope of this work.

5.3 Effect of the vehicle model used for the synthesis of the controller

As shown previously, capturing the coupling effects between car-body bending and bogie pitch is essential to a correct design of the controller for SAPS. The discussion of the results is therefore concluded providing a short comparison of the results obtained using the controller designed based on the 7-DOF coupling model and the one designed based on the

7-DOF classic model.

As an example, Fig. 16 compares the performance of the two controllers in multi-mode configuration Q_1 at speed 230 km/h and 157 km/h. At 230 km/h (left) the dominant peak in the PSD of car-body acceleration is caused by the resonance at 11.8Hz which is strongly affected by the coupling of car-body bending and bogie pitch. Since this coupling mechanism is not captured by the 7-DOF classic model, the controller designed using this model fails to mitigate car-body vibration at the resonance frequency and actually causes increased vibration compared to the passive vehicle. On the other hand, at speed 157 km/h the mechanism of excitation is due to the coupling of bogie bounce to car-body bending which is considered by both simplified models. Consistently, both controllers are able to suppress the vibrations in the interested frequency range, although the LQG based on the classic model is less effective for bending control. The difference between the two cases shows clearly that the classic 7-DOF model is only acceptable when car-body bending is excited by a mechanism involving the coupling with bogie bounce motion.

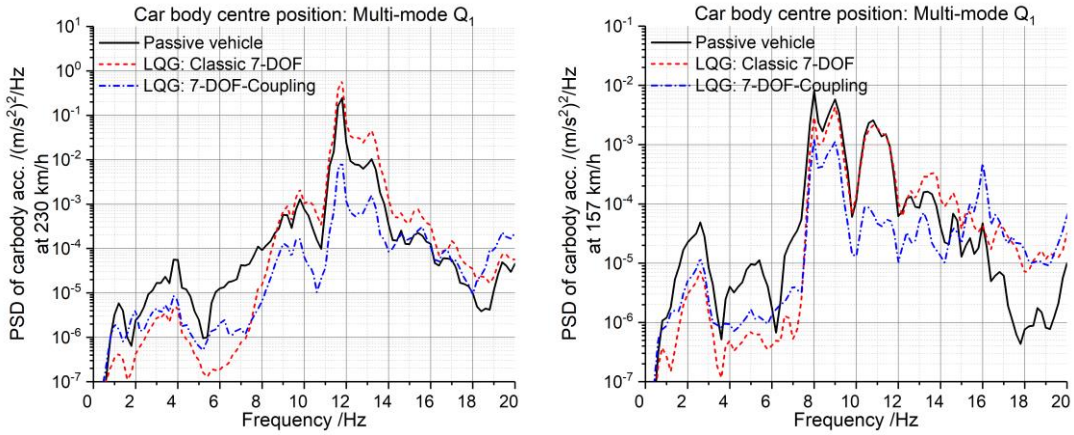

Fig. 16 Comparison of the PSD of car-body acceleration for the Multimode Q_1 LQG controller designed using the classic and Coupling 7-DOF models. Left: vehicle speed 230 km/h. Right: vehicle speed 157km/h

6 Conclusions

This paper investigated the use of semi-active primary suspensions (SAPS) to improve ride quality in a high-speed railway vehicle. A new approach to the design of a model-based controller for SAPS is introduced in this work, allowing to consider the effect of carbody-to-bogie connection through yaw dampers and traction links. This effect plays a pivotal role in determining the bending vibration of the car-body, and missing to consider this effect may result in unsuccessful design of the controller.

The design of an LQG controller for the semi-active suspension is based on a new 7-DOF-Coupling model: this model is sufficiently simple to be used as the basis for the design of the controller and for state estimation based on a Kalman filter, but is found to be much more accurate than the 'classic' 7-DOF model used in previous work [14, 16] when stiff yaw dampers and traction links are included in the vehicle's suspensions.

Different configurations of the LQG controller are assessed using co-simulation of a detailed FMBS vehicle model defined in SIMPACK and a Simulink model of the controllers and of the semi-active dampers. First, one-at-time modal control is implemented showing the benefits of controlling different components of motion in the vehicle. This analysis shows that car-body vibration in the high frequency range can be mitigated not only by directly controlling the bending mode of the car-body, but also through the control of bogie vibration, either bogie pitch or bogie bounce depending on the specific resonance of the car-body caused by the combination of vehicle speed and dominant wavelength of track irregularity. These results suggest that simpler control strategies, such as modal skyhook applied to bogie bounce and bogie pitch could also be effective towards improving ride quality in a wide range of running speeds and could be implemented using a reduced set of sensors and a simpler controller compared to model-based controllers.

Then, two multi-mode LQG controller are proposed which combine the benefits of different one-at-a-time ones and therefore allow to reduce car-body vibration in the entire frequency range of interest up to 20Hz.

Further developments of this work are envisaged to consider the effect of the controllable damper dynamics, in particular considering magneto-rheological damper as a suitable technology for this application, requiring a large pass-band of the semi-active dampers. Furthermore, improved control strategies for this application could be investigated, introducing gain scheduling to consider the fact that different modes of the vehicle are excited at different running speeds, and designing a robust controller like $H\infty$ which is the best suited to cope with parameter uncertainty affecting the railway vehicle in real service.

Declaration of interest

No potential conflict of interest was reported by the author(s).

Reference

[1] BS ISO 2631-4:2001+A1:2010. Mechanical vibration and shock-Evaluation of human exposure to whole-body vibration, (n.d.).

[2] G. Diana, F. Cheli, A. Collina, R. Corradi, S. Melzi, The Development of a Numerical Model for Railway Vehicles Comfort Assessment Through Comparison With Experimental Measurements, Veh. Syst. Dyn. 38 (2002) 165–183. https://doi.org/10.1076/vesd.38.3.165.8287.

[3] J. Zhou, R. Goodall, L. Ren, H. Zhang, Influences of car body vertical flexibility on ride quality of passenger railway vehicles, Proc. Inst. Mech. Eng. Part F J. Rail Rapid Transit. 223 (2009) 461–471. https://doi.org/10.1243/09544097JRRT272.

[4] M. Dumitriu, A new passive approach to reducing the carbody vertical bending vibration of railway vehicles, Veh. Syst. Dyn. 55 (2017) 1787–1806. https://doi.org/10.1080/00423114.2017.1330962.

[5] T. You, J. Zhou, D.J. Thompson, D. Gong, J. Chen, Y. Sun, Vibration reduction of a high-speed train floor using multiple dynamic vibration absorbers, Veh. Syst. Dyn. (2021). https://doi.org/10.1080/00423114.2021.1928248.

[6] R. Goodall, G. Freudenthaler, R. Dixon, Hydraulic actuation technology for full- and semi-active railway suspensions, Veh. Syst. Dyn. 52 (2014) 1642–1657. https://doi.org/10.1080/00423114.2014.953181.

[7] A. Qazizadeh, R. Persson, S. Stichel, On-track tests of active vertical suspension on a passenger train, Veh. Syst. Dyn. 53 (2015) 798–811. https://doi.org/10.1080/00423114.2015.1015429.

[8] E. Foo, R.M. Goodall, Active suspension control of flexible-bodied railway vehicles using electro-hydraulic and electro-magnetic actuators, Control Eng. Pract. 8 (2000) 507–518. https://doi.org/10.1016/S0967-0661(99)00188-4.

[9] C. Huang, J. Zeng, G. Luo, H. Shi, Numerical and experimental studies on the car body flexible vibration reduction due to the effect of car body-mounted equipment, Proc. Inst. Mech. Eng. Part F J. Rail Rapid Transit. 232 (2018) 103–120. https://doi.org/10.1177/0954409716657372.

[10] Q. Wang, J. Zeng, Y. Wu, B. Zhu, Study on semi-active suspension applied on carbody underneath suspended system of high-speed railway vehicle, JVC/Journal Vib. Control. 26 (2020) 671–679. https://doi.org/10.1177/1077546319889863.

[11] C. Huang, J. Zeng, Suppression of the flexible carbody resonance due to bogie instability by using a DVA suspended on the bogie frame, Veh. Syst. Dyn. (2021) 1–20. https://doi.org/10.1080/00423114.2021.1930071.

[12] D. Gong, G. Liu, J. Zhou, Research on mechanism and control methods of carbody chattering of an electric multiple-unit train, Multibody Syst. Dyn. 53 (2021) 135–172. https://doi.org/10.1007/s11044-021-09779-9.

[13] Y. SUGAHARA, T. TAKIGAMI, A. KAZATO, R. KOGANEI, M. SAMPEI, Suppression of Vertical Vibration in Railway Vehicles by Damping Force Control of Primary Suspension Using an LQG Controller, J. Syst. Des. Dyn. 2 (2008) 251–262. https://doi.org/10.1299/jsdd.2.251.

[14] Y. Sugahara, A. Kazato, R. Koganei, M. Sampei, S. Nakaura, Suppression of vertical bending and rigid-body-mode vibration in railway vehicle car body by primary and secondary suspension control: Results of simulations and running tests using Shinkansen vehicle, Proc. Inst. Mech. Eng. Part F J. Rail Rapid Transit. 223 (2009) 517–531. https://doi.org/10.1243/09544097JRRT265.

[15] Y. Sugahara, T. Takigami, R. Koganei, Suppression of Vertical Bending Vibration in Railway Car Bodies By Primary Suspension Damping Control (Results of Running Tests Using Shinkansen Vehicles), in: Proc. 21st Int. Symp. Dyn. Veh. Roads Tracks (IAVSD 2009), 2009: pp. 1–12.

[16] B. Fu, S. Bruni, An examination of alternative schemes for active and semi-active control of vertical car-body vibration to improve ride comfort, Proc. Inst. Mech. Eng. Part F J. Rail Rapid Transit. (2021) 095440972110221. https://doi.org/10.1177/09544097211022108.

[17] B. Fu, B. Liu, E. Di Gialleonardo, S. Alfi, S. Bruni, Improvement of high-speed vehicle vertical ride comfort with semi-active primary suspension Rail vehicle model, in: Proc. 27th Int. Symp. Dyn. Veh. Roads Tracks (IAVSD 2021), n.d.: pp. 1–10.

[18] T. Tomioka, T. Takigami, Reduction of bending vibration in railway vehicle carbodies using carbody–bogie dynamic interaction, Veh. Syst. Dyn. 48 (2010) 467–486. https://doi.org/10.1080/00423114.2010.490589.

[19] L.-H. Zong, X.-L. Gong, S.-H. Xuan, C.-Y. Guo, Semi-active H∞ control of high-speed railway vehicle suspension with magnetorheological dampers, Veh. Syst. Dyn. 51 (2013) 600–626. https://doi.org/10.1080/00423114.2012.758858.

[20] M. El-Kafafy, S.M. El-Demerdash, A.-A.M. Rabeih, Automotive Ride Comfort Control Using MR Fluid Damper, Engineering. 04 (2012) 179–187. https://doi.org/10.4236/eng.2012.44024.

[21] D. 3. .-S. of the art actuator technology Research report of project RUN2RAIL, No Title,

n.d.

[22] D.H. Wang, W.H. Liao, Magnetorheological fluid dampers: A review of parametric modelling, Smart Mater. Struct. 20 (2011). https://doi.org/10.1088/0964-1726/20/2/023001.

[23] J.H. Koo, F.D. Goncalves, M. Ahmadian, A comprehensive analysis of the response time of MR dampers, Smart Mater. Struct. 15 (2006) 351–358. https://doi.org/10.1088/0964-1726/15/2/015.

[24] S. Bruni, A. Collina, G. Diana, P. Vanolo, Lateral dynamics of a railway vehicle in tangent track and curve: tests and simulation, Veh. Syst. Dyn. 33 (1999) 464–477. https://doi.org/10.1080/00423114.1999.12063104.

[25] S.S. Rao, Vibration of Continuous Systems, Second Edi, Wiley, 2019. https://doi.org/10.1017/CBO9781107415324.004.

[26] S.L. Brunton, J.N. Kutz, Data-Driven Science and Engineering: Machine Learning, Dynamical Systems, and Control, Cambridge University Press, 2019. https://doi.org/10.1017/9781108380690.

[27] EN 12299, Railway applications. Ride comfort for passengers. Measurement and evaluation, (n.d.).

Appendix 1

Table A.1 parameters of the vehicle model

Symbol	Explanation	Value
M_c	Mass of car-body	40 [t]
J_c	Inertia of car-body	2×10^6 [kg· m^2]
M_t	Mass of bogie	3000 [kg]
J_t	Inertia of bogie	2000 [kg· m^2]
C_{sz}	Equivalent vertical damping of secondary suspension	2×45 [kNs/m]
K_{sz}	Equivalent vertical stiffness of secondary suspension	$2 \times$0.6 [MN/m]
C_{ed}	Equivalent longitudinal damping of yaw dampers	2×500 [kNs/m]
K_{ed}	Equivalent longitudinal stiffness of yaw dampers	2×8 [MN/m]
K_t	Stiffness of traction link	8 [MN/m]
C_{pz}	Equivalent vertical damping of primary suspension (in passive mode)	2×10 [kNs/m]
K_{pz}	Equivalent vertical stiffness of primary suspension	2×1.3 [MN/m]
H_b	Height of bogie centre of gravity	0.65 [m]
H_{cg}	Height of car-body centre of gravity	1.85 [m]
H_{cb}	Height of car-body first bending neutral layer	1.6 [m]
L_c	Car-body length	25 [m]
L_t	Half distance between two bogie centres	8.9 [m]
L_w	Half distance of wheelbase	1.25 [m]
H_t	Height of traction link	0.35 [m]
H_y	Height of yaw damper	0.4 [m]
L_1,L_2	Distance from car-body rear end to front/rear bogie centre	21.4/3.6 [m]
L_{y1},L_{y2}	Distance from car-body rear end to the front/rear yaw damper	20.86/4.14 [m]
L_{t1},L_{t2}	Distance from car-body rear end to the front/rear traction link	21.2/3.8 [m]